EurJIC European Journal of Inorganic Chemistry
ChemPubSoc Europe
FULL PAPER

DOI:10.1002/ejic.201301586

Immobilization of 1,5,7-Triazabicyclo[4.4.0]dec-5-ene on Magnetic γ-Fe_2O_3 Nanoparticles: A Highly Recyclable and Efficient Nanocatalyst for the Synthesis of Organic Carbonates

Liqiang Wu*[a] and Shuanbao Tian[b]

Keywords: Heterogeneous catalysis / Iron / Nanoparticles / Immobilization / Transesterification / Carbonates

1,5,7-Triazabicyclo[4.4.0]dec-5-ene was immobilized on magnetic γ-Fe_2O_3 nanoparticles as a magnetic nanocatalyst. The nanoparticle reagent was obtained with good loading levels and has been successfully used for the efficient and selective synthesis of organic carbonates by the direct condensation of alcohols and diethyl carbonate. The catalyst is quantitatively recovered by an external magnet and can be reused for six cycles with almost consistent activity.

Introduction

Organic carbonates are useful intermediates for the synthesis of fine chemicals,[1] pharmaceuticals,[2] plasticizers, synthetic lubricants,[3] monomers for organic glasses,[4] and solvents.[5] They are also used as linkers and tagging moieties in solid-phase chemistry.[6] The most common procedures for the synthesis of these compounds include the reaction of phosgene with diols and the coupling of halo compounds with alcohols and phenols.[7] As highly toxic and harmful reagents, such as phosgene or haloformates, are involved, most procedures for the synthesis of these compounds are not environmentally acceptable. Recently, symmetrical organic carbonates, especially dimethyl carbonate (DMC) and diethyl carbonate (DEC), have been synthesized from CO_2, epoxides, and alcohols[8] or synthesized directly from CO_2 and alcohols.[9] The synthesis of unsymmetrical organic carbonates by transesterification with alcohols has been successfully achieved by solid base catalysts, such as MCM-41-TBD,[10] Mg/La metal oxide,[11] CsF/α-Al_2O_3,[12] nanocrystalline MgO,[13] metal–organic frameworks,[14] and Bu_2SnMoO_4.[15] However, the development of highly efficient synthetic routes for the production of unsymmetrical organic carbonates is an interesting topic.

With increasing environmental concerns, the development of efficient and recoverable heterogeneous catalysts has become an important research field. In this context, nanoparticles as heterogeneous catalysts have attracted a great deal of attention owing to their interesting structures and high catalytic activities. Furthermore, nanometer-sized particles are easily dispersible in solution to form stable suspensions.[16] In spite of these advantages, the tedious recycling of such small particles by expensive ultracentrifugation has limited their application. To further address the issues of recyclability and reusability, magnetic nanoparticles (MNPs) have emerged as excellent supports that are amenable to simple magnetic separation.[17] Moreover, magnetic nanoparticles can be functionalized readily through appropriate surface modifications, and various functionalities can be loaded.[18]

As a continuation of our interest in the development of efficient and environmentally benign synthetic methodologies,[19] we report herein on the preparation of a new type of magnetically separable γ-Fe_2O_3-immobilized 1,5,7-triazabicyclo[4.4.0]dec-5-ene nanoparticles (MNPs-TBD) and their application for the synthesis of organic carbonates (Scheme 1).

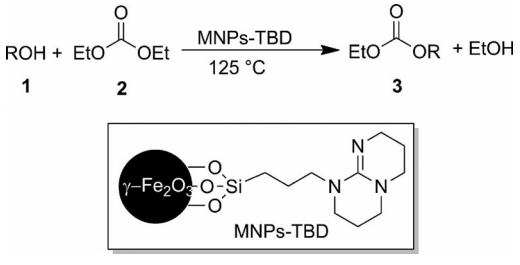

Scheme 1. Synthesis of organic carbonates by using MNPs-TBD.

[a] School of Pharmacy, Xinxiang Medical University,
East of JinSui Road of Xinxiang City, 453003 Henan Province, P. R. China
E-mail: wliq870@163.com
http://www.xxmu.edu.cn/
[b] School of Basic Medical Sciences, Xinxiang Medical University, Xinxiang 453003, P. R. China

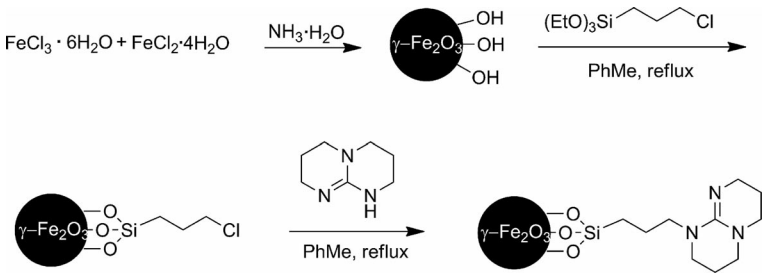

Scheme 2. Synthesis of MNPs-TBD.

Results and Discussion

γ-Fe_2O_3 nanoparticles were prepared through a chemical coprecipitation method and were subsequently coated with (3-chloropropyl)triethoxysilane to achieve 3-chloropropyl-functionalized γ-Fe_2O_3. Ultimately, the reaction of this material containing chlorine groups with 1,5,7-triazabicyclo[4.4.0]dec-5-ene led to MNPs-TBD nanoparticles (Scheme 2). The MNPs-TBD was characterized by FTIR spectroscopy, energy-dispersive spectroscopy (EDS), scanning electron microscopy (SEM), transmission electron microscopy (TEM), powder X-ray diffraction (XRD), vibrating sample magnetometery (VSM), thermogravimetric analysis (TGA), and elemental analysis. The specific surface areas of the powders were determined by use of the Brunauer–Emmett–Teller (BET) method. Unfortunately, owing to the magnetic properties of MNPs-TBD, it is impossible to further characterize this material by solid-state NMR spectroscopy.

Figure 1 shows the FTIR spectra of γ-Fe_2O_3 nanoparticles and MNPs-TBD. The FTIR spectrum of γ-Fe_2O_3 nanoparticles exhibits two characteristic peaks at 561 and 636 cm^{-1} owing to the stretching vibrations of the Fe–O bond in γ-Fe_2O_3. The FTIR spectrum of MNPs-TBD shows Fe–O vibrations in the same vicinity. Compared with the spectrum of the unfunctionalized γ-Fe_2O_3, the significant features in the spectrum of MNPs-TBD were the peaks at 2918 and 2846 (C–H stretching vibration), 1126 and 1001 (Si–O stretching vibrations), and 1628 and 1320 cm^{-1} (C=N and C–N vibrations of the TBD ring, respectively). This analysis, in combination with the microanalysis data (Figure 2), indicated the successful anchoring of the TBD groups on the surface of γ-Fe_2O_3.

The XRD pattern of MNPs-TBD shows characteristic peaks and relative intensities that match well with the cubic structure of maghemite (JCPDS file No 39–1364). Diffraction peaks at $2\theta \approx 30.62$, 35.92, 43.48, 54.00, 57.62, and 63.36, which correspond to the (220), (311), (400), (422), (511), and (440) faces, are readily recognized from the XRD pattern (Figure 3). The average crystallite size was calculated as 14.2 nm by using the Scherrer equation.

Bond formation between the nanoparticles and the catalyst can be inferred from the TGA results. TGA was also used to determine the percentage of organic functional groups chemisorbed onto the surface of the magnetic nanoparticles. The TGA curve of the MNPs-TBD shows the mass loss of the organic functional group as it decomposes upon heating (Figure 4). The weight loss below 100 °C is due to the removal of physically adsorbed water molecules.

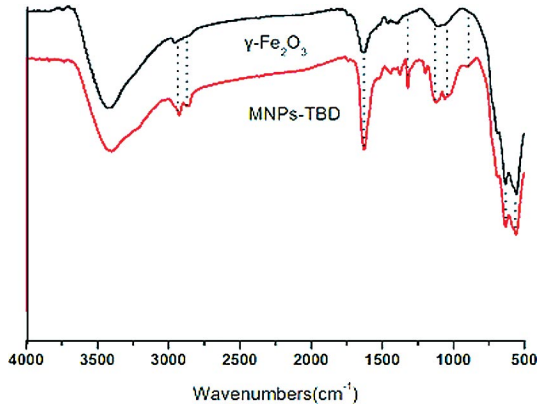

Figure 1. FTIR spectra of γ-Fe_2O_3 and MNPs-TBD.

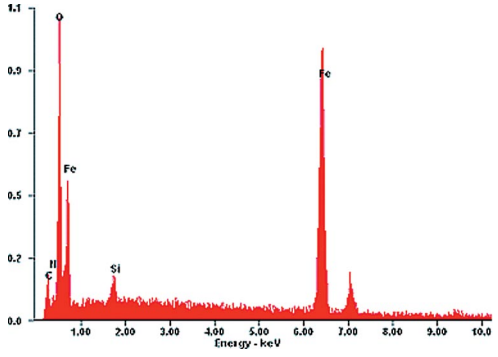

Figure 2. EDS spectrum of MNPs-TBD.

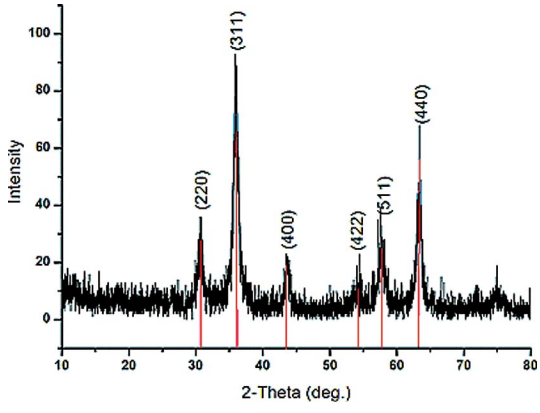

Figure 3. XRD pattern of MNPs-TBD.

Organic groups have been reported to desorb at temperatures above 250 °C. A weight loss of ca. 24.6% from 250–760 °C results from the decomposition of the organic spacer grafted to the MNPs surface. On the basis of these results, the grafting of the TBD groups on the MNPs is verified.

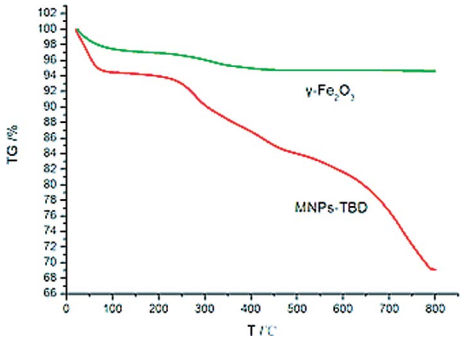

Figure 4. TGA curve of MNPs-TBD.

The shape and surface morphology of the MNPs-TBD were investigated by SEM and TEM. As shown in Figure 5, the low-magnification SEM images shows small nanosized grains with spherical and quasispherical morphology with a narrow size distribution, which indicates the nanocrystalline nature of the γ-Fe_2O_3 nanoparticles. The presence of some larger particles indicates aggregation or overlap of smaller particles. The sizes of the MNPs-TBD particles were further analyzed by TEM, and the results (Figure 6) show that the nanoparticles have dimensions ranging from 10 to 20 nm. In the TEM images, the shapes are somewhat rectangular, which is attributed to the presence of TBD groups covalently attached to the γ-Fe_2O_3 surfaces.

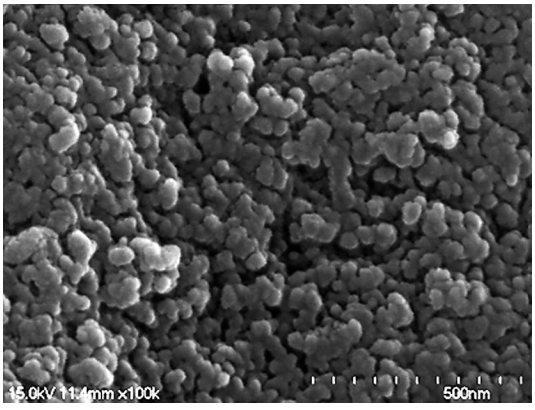

Figure 5. SEM image of MNPs-TBD.

Superparamagnetic particles are beneficial for magnetic separation, and the magnetic properties of γ-Fe_2O_3 and MNPs-TBD were characterized by VSM. The room-temperature magnetization curves of γ-Fe_2O_3 and MNPs-TBD are shown in Figure 7. As expected, the bare γ-Fe_2O_3 showed the higher magnetic value (saturation magnetization, M_s) of 61.2 emu/g, and the M_s value of MNPs-TBD is lower because the nonmagnetic material (organic ligands) on the particle surface makes a larger percentage of the mass of the particle nonmagnetic. However, this value is

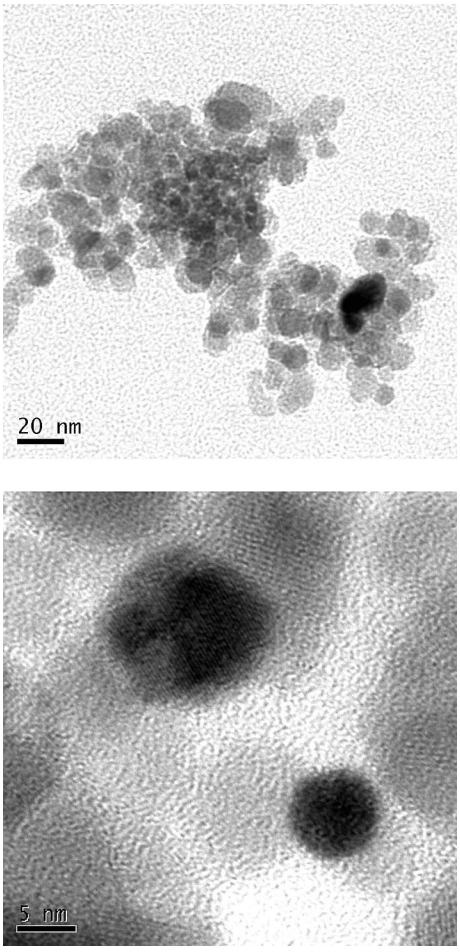

Figure 6. TEM (top) and HR-TEM (bottom) images of MNPs-TBD.

sufficiently high for magnetic separation. The strong magnetization of the nanoparticles was also revealed by simple attraction with an external magnet.

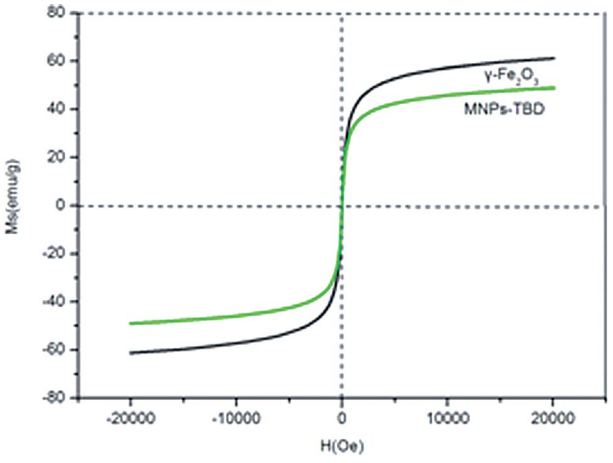

Figure 7. Magnetic curves of MNPs-TBD and γ-Fe_2O_3.

The N_2 adsorption–desorption isotherm provided a valuable tool for the study of the textural and structural properties. The specific surfaces areas of the powders were deter-

mined by use of the BET method. The BET results showed that the average surface area of γ-Fe_2O_3 was 73.79 $m^2 g^{-1}$ and that of MNPs-TBD was 29.87 $m^2 g^{-1}$ (Figure 8). γ-Fe_2O_3 had a much higher surface area than that of MNPs-BETB. This seems logical as the successful anchoring of TBD on the surface of MNPs decreases the surface area.

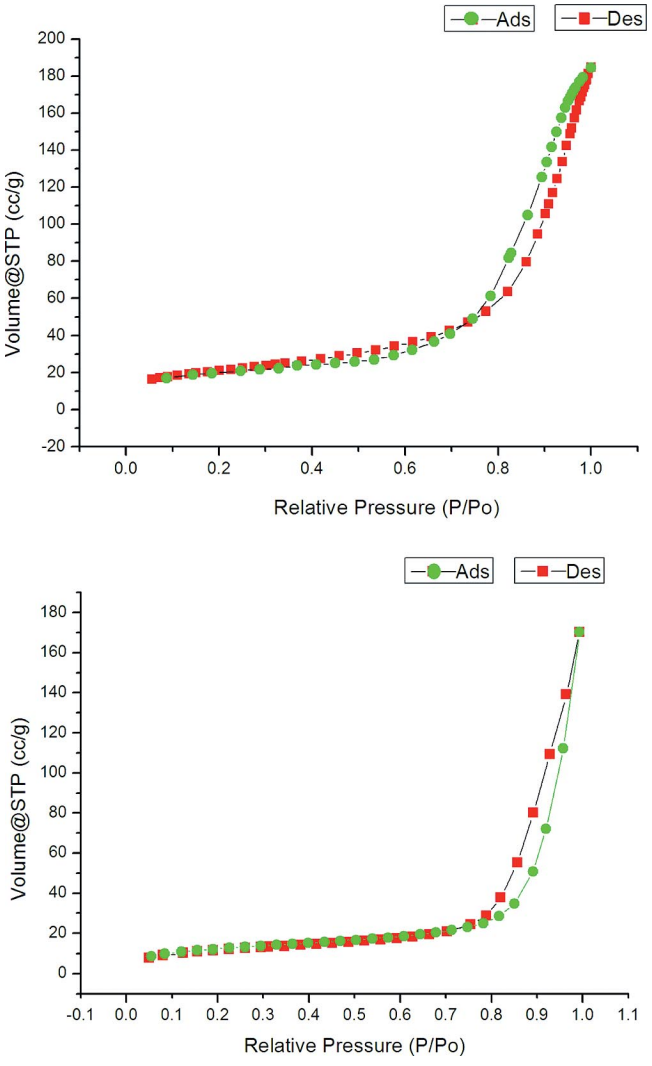

Figure 8. N_2 adsorption–desorption isotherms of γ-Fe_2O_3 (top) and MNPs-TBD (bottom).

Initially, we condensed benzyl alcohol (10 mmol) and diethyl dicarbonate (165 mmol, 20 mL). They were stirred at room temperature for 48 h in the absence of the catalyst, and very poor yields were obtained (Table 1, Entry 1). To enhance the yield of the desired product, the temperature of the reaction was increased to 125 °C, and no appreciable increment in the product yield was observed (Table 1, Entry 2). Then, we repeated the reaction in the presence of catalyst and also evaluated the amount of catalyst required for this transformation; by using 100 mg/mmol of catalyst, we obtained 82% yield. The maximum yield of 97% was obtained when the reaction was performed with 150 mg/mmol of the catalyst. Any further increase of catalyst loading does not affect the yield (Table 2, Entries 5 and 6). The reaction temperature was also examined, and 125 °C was the optimum temperature. Temperatures of less than 100 °C led to significantly decreased yields of the desired product.

Table 1. Optimization of the reaction conditions for the synthesis of benzyl ethyl carbonate.

Entry	Catalyst [mg]	*T* [°C]	Time [h]	Yield [%]
1	0	r.t.	48	0
2	0	125	20	trace
3	100	125	10	82
4	150	125	10	97
5	200	125	10	94
6	250	125	10	95
7	150	100	10	69
8	150	110	10	86
9	150	120	10	91

In an effort to understand the scope of the reaction, the reactivity of a variety of alcohols, including alkyl, cyclic, heterocyclic, aryl, and diols, with diethyl dicarbonate in the presence of the best catalytic system was investigated (Table 2). All of the substrates were selectively transformed to the corresponding unsymmetrical carbonates in quantitative yields; disubstituted symmetric carbonates were not formed in the reactions. Notably, 1,2-diols led to the formation of cyclic carbonates (Table 2, Entries 13–15), whereas cyclic products were not formed when the number of methylene groups between the alcohol functions increased. Thus, 2,5-hexanediol and 1,4-cyclohexanediol yielded the corresponding biscarbonates as the sole reaction products (Table 2, Entries 16 and 17).

A plausible mechanism could be represented by a typical transesterification process; it is hypothesized that the present transformation may have resulted from the catalytic cycle depicted in Scheme 3. MNPs-TBD is sufficiently nucleophilic to attack the carbonyl group of diethyl carbonate to afford the MNPs-TBD salt. Subsequent attack of the alcohol on the activated carbonyl group of the MNPs-TBD salt gives the product and restores the catalyst. This step is particularly favored as the positive charge, delocalized over the three nitrogen atoms, promotes the nucleophilic attack of the carbonyl by enhancing its electrophilic character.

The feasibility of repeated use of MNPs-TBD was also investigated for the reaction of benzyl alcohol with diethyl dicarbonate. This catalyst demonstrated excellent recyclability. The catalyst can be efficiently recovered easily and rapidly from the product by exposure to an external magnet (Figure 9). To remove the residual product, the remaining magnetic nanoparticles were further washed with EtOH, air-dried, and used directly for the next reaction without further purification. The recycled catalyst was used for up to six runs with little loss of activity (Figure 10). After the catalyst was recycled, the nanocatalyst particle size and morphology have no significant changes, and the loading amount of the catalyst decreased to 0.652 mmol/g on the basis of TEM and TGA results (Figure 11). However, the activity of the catalyst showed no significant loss.

Table 2. Preparation of unsymmetrical organic carbonates.

Entry	Alcohol	Product	Time [h]	Yield [%]	Ref.
1	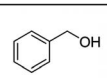	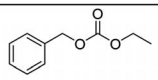 **3a**	10	97	[13]
2	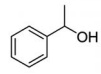	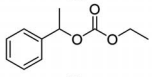 **3b**	6	98	[13]
3	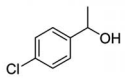	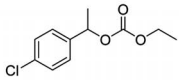 **3c**	6	98	[13]
4	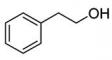	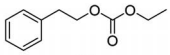 **3d**	10	93	[15]
5	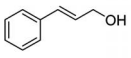	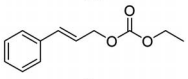 **3e**	6	95	[12]
6		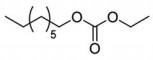 **3f**	3	99	[12]
7		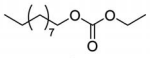 **3g**	3	99	[15]
8		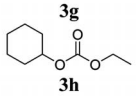 **3h**	10	92	[15]
9		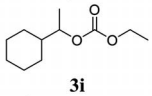 **3i**	6	96	[13]
10		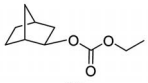 **3j**	3	98	[13]
11		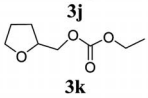 **3k**	10	93	[13]
12	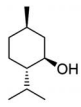	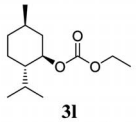 **3l**	4	99	[13]
13	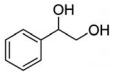	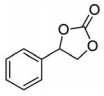 **3m**	10	95	[12]
14	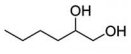	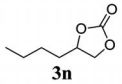 **3n**	4	99	[12]
15	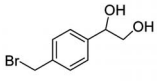	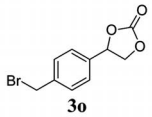 **3o**	5	97	
16		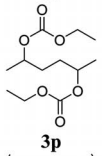 **3p**	8	95	[12]
17	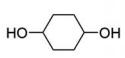	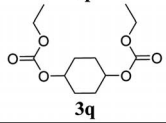 **3q**	10	94	[12]

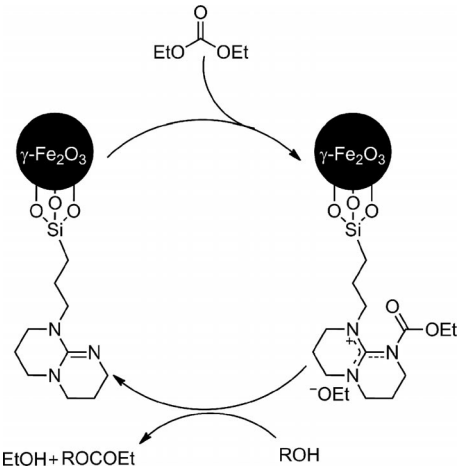

Scheme 3. A plausible mechanism for the reaction.

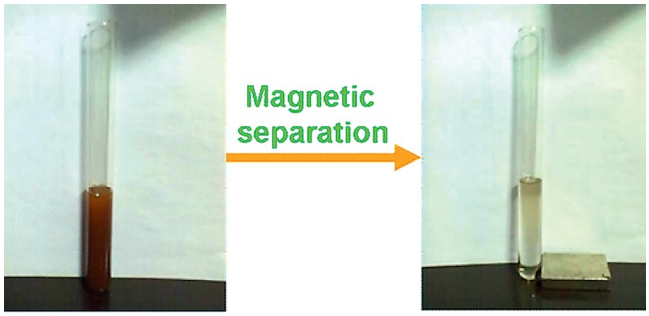

Figure 9. Left: reaction mixture containing MNPs-TBD. Right: MNPs-TBD collected by using an external magnet after the reaction.

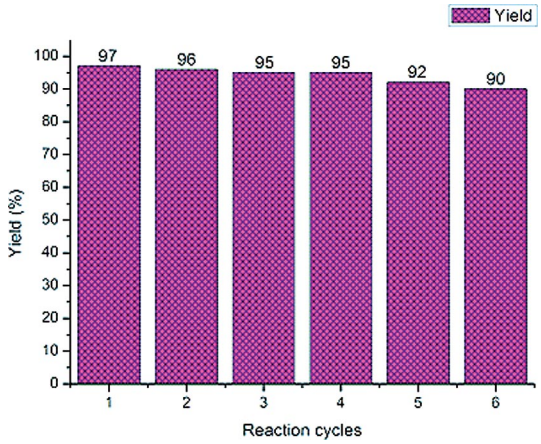

Figure 10. Recycling experiments for the synthesis of benzyl ethyl carbonate.

To demonstrate the merit of the present work, we compared the results of the synthesis of benzyl ethyl carbonate in the presence of various catalysts. Only 5% of the target compound, benzyl ethyl carbonate, was obtained in the presence of γ-Fe_2O_3 nanoparticles. When this reaction was performed with inorganic bases such as Na_2CO_3 and K_2CO_3, only trace amounts of the expected product were obtained. In the presence of organic bases such as 1,4-di-

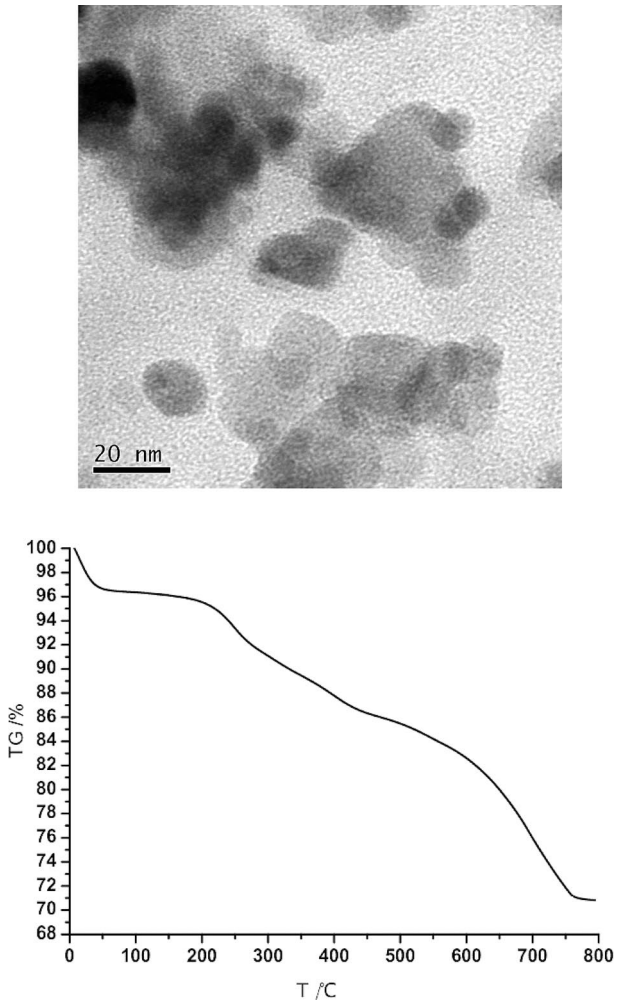

Figure 11. TEM image (top) and TGA curve (bottom) of recycled MNPs-TBD.

azabicyclo[2.2.2]octane (DABCO), 1,8-diazabicyclo[5.4.0]-undec-7-ene (DBU), and TBD, the product was obtained in low yield. The best result was obtained by using MNPs-TBD as the catalyst (Table 3). These results confirm that the inorganic support can influence the catalyst efficiency. As a strong base, the supported TBD is sufficiently nucleophilic to attack the carbonyl group of diethyl carbonate to produce the guanidinium salt. Of course, an EtO^- counterion may be the actual basic catalyst, and some reactions were performed to test this hypothesis. However, benzyl ethyl carbonate is only produced in traces in the presence of EtONa, which suggests that the ethoxide ion is not the catalyst. However, by using a guanidinium salt such as [TBD][Ac], benzyl ethyl carbonate was obtained in 56% yield; therefore, the catalyst may be present in the reaction mixture as *N*-carbethoxyguanidinium.

Table 3. Synthesis of benzyl ethyl carbonate by using various catalysts.

Entry	Catalyst	Time [h]	Yield [%]
1	nano γ-Fe_2O_3	24	5
2	Na_2CO_3	24	trace
3	K_2CO_3	24	trace
4	DABCO	10	27
5	DBU	10	26
6	TBD	10	38
7	EtONa	10	trace
8	[TBD][Ac]	10	56
9	MNPs-TBD	10	97

Conclusions

We have synthesized the first MNPs-TBD for use as a magnetic heterogeneous basic nanocatalyst. The catalyst is easily synthesized and can catalyze the synthesis of organic carbonates with good-to-high yields under different conditions. The characteristic aspects of this catalyst are its rapid, simple, and efficient separation by an appropriate external magnet; this minimizes the catalyst loss during separation, and the catalyst is reusable several times with little loss of activity. In addition, MNPs-TBD couples the advantages of heterogeneous and homogeneous TBD-based systems, which make it a promising material for industrial applications.

Experimental Section

General: Powder X-ray diffraction (XRD) patterns were recorded by using a Cu-K_α radiation source with a Bruker D8 Advance powder diffractometer. Scanning electron microscopy (SEM) studies were conducted with an Inspect F50 scanning electron microscope. Transmission electron microscopy (TEM) studies were performed by using an FEI Tecnai G2 20 transmission electron microscope at an accelerating voltage of 150 kV. Elemental compositions were determined with a Hitachi S-4800 scanning electron microscope equipped with an energy-dispersive X-ray analysis (EDAX) spectrometer (SEM-EDS). Magnetic measurements of particles were performed by using a vibrating sample magnetometer (MPMS-XL-7). N_2 adsorption–desorption isotherms were measured by using a NOVOE 4000/TriStar II 3020 instrument at liquid nitrogen temperature (77 K). The specific surface areas were calculated from the BET equation. Thermogravimetric analysis was performed under nitrogen by using a DT-40 thermoanalyzer. IR spectra were determined with a FTS-40 infrared spectrometer. NMR spectra were recorded with a Bruker AV-400 spectrometer at room temperature with tetramethylsilane (TMS) as an internal standard; coupling constants (*J*) were measured in Hz. Elemental analyses were performed with a Vario-III elemental analyzer. Melting points were determined with a XT-4 binocular microscope. All solvents used were strictly dried according to standard operations and stored over 4A molecular sieves. All other chemicals (AR grade) were obtained from commercial resources and used without further purification. All products were characterized by comparison of their spectral and physical data with those previously reported. The reaction progress was monitored by TLC.

Large-Scale Preparation of Magnetic γ-Fe_2O_3 Nanoparticles: $FeCl_2{\cdot}4H_2O$ (9.25 mmol) and $FeCl_3{\cdot}6H_2O$ (15.8 mmol) were dissolved in deionized water (150 mL) under an Ar atmosphere at room temperature. A NH_4OH solution (25%, 50 mL) was then added dropwise to the stirring mixture at room temperature to increase the reaction pH to 11. The resulting black dispersion was continuously stirred for 1 h at room temperature and then heated to reflux for 1 h to yield a brown dispersion. The magnetic nano-

particles were then purified by a repeated centrifugation, decantation, and redispersion cycle (three times). The as-synthesized sample was heated to 200 °C at 2 °C/min and then kept in the furnace for 3 h to give a reddish-brown powder.

Preparation of MNPs-TBD: We prepared MNPs-TBD similarly to the SiO_2-TBD first prepared by Polo and co-workers.[20] A mixture of γ-Fe_2O_3 (5.0 g) and (3-chloropropyl)triethoxysilane (5.0 mL, 42.5 mmol) were added to toluene (50 mL), and the mixture was stirred at room temperature for 15 min and then heated to reflux for 24 h. The mixture was cooled to room temperature, and the products were sedimented with a magnet, washed successively with dry toluene (50 mL), and then dried under reduced pressure at 100 °C for 8 h. The loading amount of the intermediate materials functionalized with chloropropyl groups was determined to be 0.723 mmol/g by elemental analysis.

This material containing chlorine groups (5 g) was then was dispersed in dry toluene (50 mL) by sonication for 1 h, and a solution of 1,5,7-triazabicyclo[4.4.0]dec-5-ene (0.5 g) in toluene (20 mL) was then added. The reaction mixture was heated to reflux under nitrogen gas for 1 d. After this time, the solid was collected by using a permanent magnet, and it was washed with toluene (3 × 20 mL) and dichloromethane (3 × 20 mL) and dried at room temperature for 24 h. The loading amount of the catalyst was determined to be 0.705 mmol/g by elemental analysis and TGA.

General Procedure for the Synthesis of Unsymmetrical Organic Carbonates with MNPs-TBD: A mixture of the alcohol (10 mmol), diethyl dicarbonate (20 mL), and MNPs-TBD (150 mg) was stirred at 125 °C for 3–10 h. After cooling to room temperature, MNPs-BETB was collected at the side of the flask by using a small magnet, and the residual diethyl dicarbonate were removed under reduced pressure. The crude product was chromatographed on silica gel with a mixture of hexane/ethyl acetate (80:20) as eluent.

3a: ^{1}H NMR (400 MHz, $CDCl_3$): δ = 7.39–7.30 (m, 5 H), 5.22 (s, 2 H), 4.22–4.18 (m, 2 H), 1.33 (t, J = 7.2 Hz, 3 H) ppm. ^{13}C NMR (100 MHz, $CDCl_3$): δ = 155.4, 136.3, 129.0, 128.6, 128.1, 70.3, 64.5, 14.5 ppm. $C_{10}H_{12}O_3$ (180.20): calcd. C 66.65, H 6.71; found C 66.58, H 6.75.

3b: ^{1}H NMR (400 MHz, $CDCl_3$): δ = 7.38–7.28 (m, 5 H), 5.36 (q, J = 7.0 Hz, 1 H), 4.23–4.19 (m, 2 H), 1.59 (t, J = 7.0 Hz, 3 H), 1.33 (t, J = 7.2 Hz, 3 H) ppm. ^{13}C NMR (100 MHz, $CDCl_3$): δ = 155.3, 136.8, 128.9, 128.5, 127.6, 72.0, 64.3, 21.5, 14.1 ppm. $C_{11}H_{14}O_3$ (194.23): calcd. C 68.02, H 7.27; found C 67.97, H 7.32.

3c: ^{1}H NMR (400 MHz, $CDCl_3$): δ = 7.37–7.26 (m, 4 H), 5.60 (q, J = 7.0 Hz, 1 H), 4.38–4.17 (m, 2 H), 1.58 (t, J = 7.0 Hz, 3 H), 1.33 (t, J = 7.2 Hz, 3 H) ppm. ^{13}C NMR (100 MHz, $CDCl_3$): δ = 154.9, 140.1, 134.6, 128.9, 128.0, 75.6, 64.4, 22.3, 14.2 ppm. $C_{11}H_{13}ClO_3$ (228.67): calcd. C 57.78, H 5.73; found C 57.84, H 5.75.

3d: ^{1}H NMR (400 MHz, $CDCl_3$): δ = 7.36–7.27 (m, 5 H), 4.38 (t, J = 7.2 Hz, 2 H), 4.25–4.18 (m, 2 H), 2.98 (t, J = 7.2 Hz, 2 H), 1.31 (t, J = 7.0 Hz, 3 H) ppm. ^{13}C NMR (100 MHz, $CDCl_3$): δ = 155.0, 138.6, 128.9, 128.0, 126.9, 74.8, 64.2, 33.8, 14.2 ppm. $C_{11}H_{14}O_3$ (194.23): calcd. C 68.02, H 7.27; found C 68.07, H 7.25.

3e: ^{1}H NMR (400 MHz, $CDCl_3$): δ = 7.36–7.23 (m, 5 H), 6.59 (d, J = 15.6 Hz, 1 H), 6.33 (dt, J = 5.7, 15.6 Hz, 1 H), 4.38 (t, J = 5.7 Hz, 2 H), 4.23–4.18 (m, 2 H), 1.31 (t, J = 7.0 Hz, 3 H) ppm. ^{13}C NMR (100 MHz, $CDCl_3$): δ = 155.2, 135.9, 132.3, 128.7, 128.2, 126.9, 124.5, 72.9, 64.4, 14.2 ppm. $C_{12}H_{14}O_3$ (206.24): calcd. C 69.88, H 6.84; found C 70.02, H 6.79.

3f: ^{1}H NMR (400 MHz, $CDCl_3$): δ = 4.22–4.11 (m, 4 H), 1.73–1.65 (m, 2 H), 1.44–1.26 (m, 13 H), 0.87 (t, J = 7.2 Hz, 3 H) ppm. ^{13}C NMR (100 MHz, $CDCl_3$): δ = 155.0, 70.3, 64.5, 31.8, 29.5, 29.4, 28.6, 26.3, 22.3, 14.3, 14.0 ppm. $C_{11}H_{22}O_3$ (202.29): calcd. C 65.31, H 10.96; found C 65.33, H 11.02.

3g: ^{1}H NMR (400 MHz, $CDCl_3$): δ = 4.25–4.12 (m, 4 H), 1.74–1.63 (m, 2 H), 1.46–1.27 (m, 17 H), 0.88 (t, J = 7.2 Hz, 3 H) ppm. ^{13}C NMR (100 MHz, $CDCl_3$): δ = 155.2, 70.9, 64.3, 32.0, 29.8, 29.7, 29.4, 29.3, 28.6, 26.2, 22.3, 14.4, 14.1 ppm. $C_{13}H_{26}O_3$ (230.35): calcd. C 67.79, H 11.38; found C 67.86, H 11.29.

3h: ^{1}H NMR (400 MHz, $CDCl_3$): δ = 4.23–4.18 (m, 2 H), 3.88–3.83 (m, 1 H), 1.82–1.76 (m, 2 H), 1.56–1.37 (m, 8 H), 1.33 (t, J = 7.2 Hz, 3 H) ppm. ^{13}C NMR (100 MHz, $CDCl_3$): δ = 155.2, 80.3, 64.8, 32.9, 28.3, 22.3, 14.1 ppm. $C_9H_{16}O_3$ (172.22): calcd. C 62.77, H 9.36; found C 62.83, H 9.33.

3i: ^{1}H NMR (400 MHz, $CDCl_3$): δ = 4.60–4.12 (m, 3 H), 1.95–1.44 (m, 5 H), 1.35–1.06 (m, 12 H) ppm. ^{13}C NMR (100 MHz, $CDCl_3$): δ = 155.3, 79.8, 64.7, 43.0, 28.4, 27.4, 25.9, 18.7, 14.2 ppm. $C_{11}H_{20}O_3$ (200.28): calcd. C 65.97, H 10.07; found C 65.88, H 10.01.

3j: ^{1}H NMR (400 MHz, $CDCl_3$): δ = 4.53 (d, J = 7.0 Hz, 1 H), 4.22–4.15 (m, 2 H), 2.41 (d, J = 4.4 Hz, 1 H), 2.31–2.26 (m, 1 H), 1.75–1.40 (m, 5 H), 1.32 (t, J = 7.2 Hz, 3 H), 1.22–1.08 (m, 2 H) ppm. ^{13}C NMR (100 MHz, $CDCl_3$): δ = 155.3, 80.4, 64.3, 43.3, 40.3, 36.8, 36.0, 30.8, 23.9, 14.2 ppm. $C_{10}H_{16}O_3$ (184.23): calcd. C 65.19, H 8.75; found C 65.23, H 8.70.

3k: ^{1}H NMR (400 MHz, $CDCl_3$): δ = 4.25–3.76 (m, 7 H), 2.11–1.86 (m, 3 H), 1.75–1.55 (m, 1 H), 1.30 (t, J = 7.2 Hz, 3 H), ppm. ^{13}C NMR (100 MHz, $CDCl_3$): δ = 155.1, 76.9, 69.8, 68.5, 64.3, 27.9, 25.8, 14.3 ppm. $C_8H_{14}O_4$ (174.20): calcd. C 55.16, H 8.10; found C 55.11, H 8.07.

3l: ^{1}H NMR (400 MHz, $CDCl_3$): δ = 4.51 (td, J = 4.4, 11.4 Hz, 1 H), 4.23–4.17 (m, 2 H), 2.10–2.05 (m, 1 H), 1.99–1.92 (m, 1 H), 1.82–0.86 (m, 19 H) ppm. ^{13}C NMR (100 MHz, $CDCl_3$): δ = 155.2, 79.3, 64.7, 46.8, 39.4, 33.6, 28.7, 25.6, 22.4, 21.3, 20.9, 14.1 ppm. $C_{13}H_{24}O_3$ (228.33): calcd. C 68.38, H 10.59; found C 68.43, H 10.55.

3m: ^{1}H NMR (400 MHz, $CDCl_3$): δ = 7.44–7.23 (m, 5 H), 5.65 (t, J = 8.0 Hz, 1 H), 4.81 (t, J = 8.0 Hz, 1 H), 4.33 (t, J = 8.0 Hz, 1 H) ppm. ^{13}C NMR (100 MHz, $CDCl_3$): δ = 155.1, 135.9, 129.5, 128.9, 126.7, 71.4 ppm. $C_9H_8O_3$ (164.16): calcd. C 65.85, H 4.91; found C 65.92, H 4.88.

3n: ^{1}H NMR (400 MHz, $CDCl_3$): δ = 4.81–4.64 (m, 1 H), 4.50 (t, J = 8.0 Hz, 1 H), 4.12 (dd, J = 7.2, 8.0 Hz, 1 H), 2.02–1.22 (m, 6 H), 0.97 (t, J = 7.2 Hz, 3 H) ppm. ^{13}C NMR (100 MHz, $CDCl_3$): δ = 155.6, 76.9, 69.2, 33.7, 26.5, 22.8, 14.2 ppm. $C_7H_{12}O_3$ (144.17): calcd. C 58.32, H 8.39; found C 58.36, H 8.32.

3o: ^{1}H NMR (400 MHz, $CDCl_3$): δ = 7.50–7.39 (m, 4 H), 5.64 (t, J = 8.0 Hz, 1 H), 4.79 (dd, J = 7.6, 8.4 Hz, 1 H), 4.62 (s, 2 H), 4.36 (t, J = 7.6, 8.4 Hz, 3 H) ppm. ^{13}C NMR (100 MHz, $CDCl_3$): δ = 156.8, 139.1, 136.4, 130.4, 126.4, 78.3, 69.8, 43.7 ppm. $C_{10}H_9BrO_3$ (257.08): calcd. C 46.72, H 3.53; found C 46.77, H 3.49.

3p: ^{1}H NMR (400 MHz, $CDCl_3$): δ = 4.85–4.69 (m, 2 H), 4.22–4.17 (m, 4 H), 1.81–1.56 (m, 4 H), 1.33 (t, J = 7.0 Hz, 6 H) ppm. ^{13}C NMR (100 MHz, $CDCl_3$): δ = 154.9, 75.1, 74.5, 63.9, 32.0, 31.5, 20.2, 19.8, 14.3 ppm. $C_{16}H_{22}O_6$ (310.35): calcd. C 54.95, H 8.45; found C 55.02, H 8.42.

3q: ^{1}H NMR (400 MHz, $CDCl_3$): δ = 4.78–4.65 (m, 2 H), 4.22–4.18 (m, 4 H), 2.11–1.56 (m, 8 H), 1.33 (t, J = 7.0 Hz, 6 H) ppm. ^{13}C NMR (100 MHz, $CDCl_3$): δ = 154.7, 74.7, 73.8, 63.9, 63.7, 27.7. 27.4, 14.3 ppm. $C_{12}H_{20}O_6$ (260.29): calcd. C 55.37, H 7.74; found C 55.42, H 7.69.

Acknowledgments

The authors are pleased to acknowledge financial support from the Scientific Research Fund of Xinxiang Medical University (grant number 2013QN130).

[1] Y. Ono, *Appl. Catal. A* **1997**, *155*, 133–166.
[2] J. P. Parrish, R. N. Salvatore, K. W. Jung, *Tetrahedron* **2000**, *56*, 8207–8237.
[3] S. Gryglewicz, F. A. Oko, G. Gryglewicz, *Ind. Eng. Chem. Res.* **2003**, *42*, 5007–5010.
[4] K. Takamatsu, T. Matsushita, JP 2003277327, **2003**.
[5] F. Mizia, F. Rivetti, US 20020056468, **2002**.
[6] B. Sauerbrei, V. Jungmann, H. Waldmann, *Angew. Chem. Int. Ed.* **1998**, *37*, 1143–1146; *Angew. Chem.* **1998**, *110*, 1187.
[7] a) G. Bertolini, G. Pavich, B. Vergani, *J. Org. Chem.* **1998**, *63*, 6031–6034; b) A. R. Choppin, J. W. Rogers, *J. Am. Chem. Soc.* **1948**, *70*, 2967.
[8] a) Y. Kishimoto, I. Ogawa, *Ind. Eng. Chem. Res.* **2004**, *43*, 8155–8162; b) B. M. Bhanage, S. I. Fujita, Y. Ikushima, K. Torii, M. Arai, *Green Chem.* **2003**, *5*, 71–75; c) J.-S. Tian, C.-X. Miao, J.-Q. Wang, F. Cai, Y. Du, Y. Zhao, L.-N. He, *Green Chem.* **2007**, *9*, 566–571.
[9] S. Fujita, B. M. Bhanage, Y. Ikushima, M. Arai, *Green Chem.* **2001**, *3*, 87–91.
[10] S. Carloni, D. E. De Vos, P. A. Jacobs, R. Maggi, G. Sartori, R. Sartorio, *J. Catal.* **2002**, *205*, 199–204.
[11] B. Veldurthy, F. Figueras, *Chem. Commun.* **2004**, 734–735.
[12] B. Veldurthy, J. M. Clacens, F. Figueras, *Eur. J. Org. Chem.* **2005**, 1972–1976.
[13] M. L. Kantam, U. Pal, B. Sreedhar, B. M. Choudary, *Adv. Synth. Catal.* **2007**, *349*, 1671–1675.
[14] Y.-X. Zhou, S.-G. Liang, J.-L. Song, T.-B. Wu, S.-Q Hu, H.-Z. Liu, B.-X. Han, *Acta Phys.-Chim. Sin.* **2010**, *26*, 939–945.
[15] J. L. Song, B. B. Zhang, T. B. Wu, G. Y. Yang, B. X. Han, *Green Chem.* **2011**, *13*, 922–927.
[16] V. Polshettiwar, R. S. Varma, *Green Chem.* **2010**, *12*, 743–754.
[17] a) S. Shylesh, V. Schunemann, W. R. Thiel, *Angew. Chem. Int. Ed.* **2010**, *49*, 3428–3459; *Angew. Chem.* **2010**, *122*, 3504; b) Y. H. Zhu, L. P. Stubbs, F. Ho, R. Z. Liu, C. P. Ship, J. A. Maguire, N. S. Hosmane, *ChemCatChem* **2010**, *2*, 365–374; c) T. Q. Zeng, W. W. Chen, C. M. Cirtiu, A. Moores, G. H. Song, C. J. Li, *Green Chem.* **2010**, *12*, 570–573.
[18] a) A. Megia-Fernandez, M. Ortega-Munoz, J. Lopez-Jaramillo, F. Hernandez-Mateo, F. Santoyo-Gonzalez, *Adv. Synth. Catal.* **2010**, *352*, 3306–3320; b) B. G. Wang, B. C. Ma, Q. O. Wang, W. Wang, *Adv. Synth. Catal.* **2010**, *352*, 2923–2928; c) H. Firouzabadi, N. Iranpoor, M. Gholinejad, J. Hoseini, *Adv. Synth. Catal.* **2011**, *353*, 125–132; d) A. J. Amali, R. K. Rana, *Green Chem.* **2009**, *11*, 1781–1786; e) R. L. Oliveira, P. K. Kiyohara, L. M. Rossi, *Green Chem.* **2010**, *12*, 144–149; f) R. Luque, A. Fihri, H. Zhu, J. M. Basset, *Chem. Rev.* **2011**, *111*, 3036–3075; g) S. E. García-Garrido, J. Francos, V. Cadierno, J. M. Basset, V. Polshettiwar, *ChemSusChem* **2011**, *4*, 104–111.
[19] L. Q. Wu, Z. K. Yin, *Eur. J. Inorg. Chem.* **2013**, 6156–6163.
[20] A. P. Polo, V. R. S. Quiteria, A. C. Canos, H. G. Gomez, R. J. Marin, EP 2036884, **2009**.

Received: December 18, 2013
Published Online: March 11, 2014

